Accurate noncontact calibration of colloidal probe sensitivities in atomic force microscopy

Koo-Hyun Chung, Gordon A. Shaw, and Jon R. Pratt[a)]
National Institute of Standards and Technology, Gaithersburg, Maryland 20899, USA

(Received 10 February 2009; accepted 16 May 2009; published online 15 June 2009)

The absolute force sensitivities of colloidal probes comprised of atomic force microscope, or AFM, cantilevers with microspheres attached to their distal ends are measured. The force sensitivities are calibrated through reference to accurate electrostatic forces, the realizations of which are described in detail. Furthermore, the absolute accuracy of a common AFM force calibration scheme, known as the thermal noise method, is evaluated. It is demonstrated that the thermal noise method can be applied with great success to colloidal probe calibration in air and in liquid to yield force measurements with relative standard uncertainties below 5%. Techniques to combine the electrostatics-based determination of the AFM force sensitivity with measurements of the colloidal probe's thermal noise spectrum to compute noncontact estimates of the displacement sensitivity and spring constant are also developed. [DOI: 10.1063/1.3152335]

I. INTRODUCTION

Atomic force microscopes (AFMs) (Ref. 1) can operate in force spectroscopy modes that provide insights into the mechanical properties of materials[2] while measuring physical,[3] chemical,[4] and biological[5] force interactions that occur between the tip of the AFM cantilever and the sample surface. In some instances, spherical particles are attached to the cantilever to achieve specific surface properties and a controlled geometry.[4,6] The AFM cantilever is then referred to as a colloidal probe, and is used to study interfacial phenomena in air as well as in liquid environments, such as Casimir forces,[3] surface forces,[7,8] and the mechanical properties of various materials, such as biological cells.[9] In order for microscopists to use colloidal probes to make accurate measurements, the colloidal probe sensitivity to forces and displacements must be calibrated.

Most AFMs use an optical lever scheme[10,11] that bounces light off the back of the cantilever spring onto a position sensitive photodetector (PSD). Angular displacements of the cantilever spring due to forces and moments applied at the tip cause changes in the illuminated position of the reflected beam on a PSD, which are recorded as changes in the optical lever voltage V_{OL}. Numerous methods have been developed for the calibration of V_{OL} so that the voltage represents either the force or the vertical displacement (or both) occurring at the cantilever tip. The optical lever displacement sensitivity (OLDS) in the direction normal to the sample is most often determined by recording V_{OL} as a function of the distance moved by the AFM piezoscanner when the cantilever is pressed against a rigid surface. The resulting voltage versus distance curve has a linear slope OLDS, expressed in units of V/m. The optical lever force sensitivity (OLFS) in units of V/N in the direction normal to the sample is then simply

$$\mathrm{OLFS} = \frac{\mathrm{OLDS}}{k}, \tag{1}$$

where k is the stiffness of the cantilever in the direction normal to the sample surface expressed in units of N/m. When the spring constant is measured in a coordinate system normal to the sample surface rather than normal to the flat surface of the cantilever, it is sometimes referred to as the "effective" spring constant of the system (see, for instance, Ref. 12), but will be referred to simply as the spring constant hereafter. To avoid confusion, we point out now that all sensitivities and stiffness values considered in this paper are evaluated along the direction normal to the sample surface.

The accurate calibration of the cantilever spring constant has been the subject of numerous publications and review articles, and though many useful techniques have been identified, few have proven well suited for the special case of a colloidal probe. Theoretical spring constant determinations based on beam theory or finite element modeling (see Ref. 13 for a review) might be attempted, but the effect of the adhesive used to attach the colloidal particle[14] will be difficult to capture. Reference cantilever approaches that are receiving attention as possible standards[13,15–21] and related techniques based on piezoresistive cantilevers[22] would appear more promising, since they provide a direct measurement that is based on the ratio of OLDS values determined against a rigid substrate and a known reference cantilever. Unfortunately, the friction between the colloid particle and the sample is known to be a large contributing factor[23–28] when measuring the OLDS against a rigid substrate, and seems to confound the measurement of both the necessary slopes, as illustrated in Fig. 1.

To minimize the influence of friction and to prevent damage to colloidal probes that have been chemically treated,[29–31] a noncontact method for calibrating the colloidal probe is desirable. The force of hydrodynamic drag[14] has been proposed and has demonstrated precision around 15%. The stiffness has also been determined from the resonant

a)Author to whom correspondence should be addressed. Tel.: +1-301-975-5470. FAX: +1-301-869-3536. Electronic mail: jon.pratt@nist.gov.

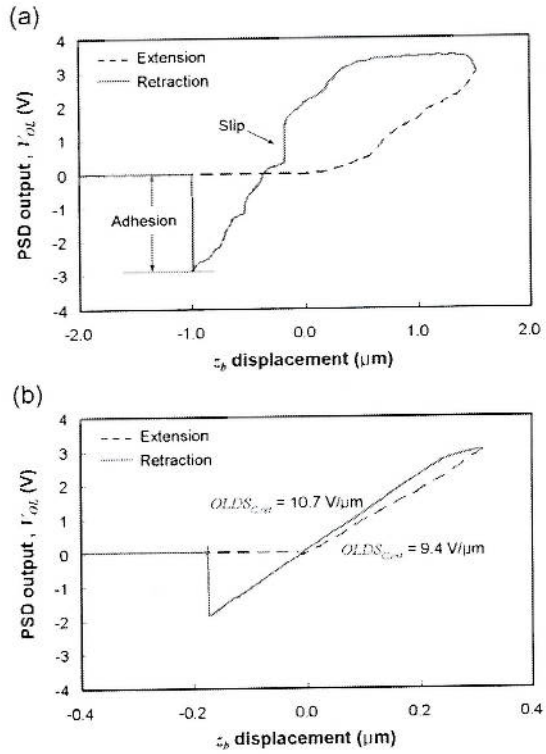

FIG. 1. (Color online) Representative calibration curves obtained by scanning a colloidal probe against (a) a reference cantilever and (b) a rigid surface. Nominal spring constant of the colloidal probe is 0.1 N/m and the spring constant of the reference cantilever as calibrated by the NIST EFB is 0.2099 N/m. A large adhesion force due to the large contact area of the colloidal probe is observed, as well as a variety of stick-slip type events. Dashed line and solid line denote extension toward and retraction away from the measurement surface, respectively.

frequency, quality factor, geometry, and the properties of the fluid in which the probe is immersed, using a nondimensional function of the Reynold's number.[32] A common technique for noncontact calibration of colloidal probes is the added mass approach,[33] where relative precision is usually estimated to be around 20%. Finally, techniques based on the equipartition theorem, or thermal noise, (e.g., Ref. 34) could be used that require only a calibrated displacement signal. Thermal noise techniques have been compared in preliminary studies to Système International d'Unités (SI) traceable references[19,35] and can, in principle, yield results in a totally noncontact fashion.[36,37] However, in order to obtain a relative accuracy beyond tens of percent the user must compute correction factors that are derived from analytical considerations of the cantilever dynamic mode shape[38] and the laser spot diameter and position along the cantilever.[39] These correction factors are as yet unknown for colloidal probes.

With this background as motivation, we propose a new noncontact calibration method using electrostatic forces. Here, the OLFS of an electrically conductive probe is obtained by applying an accurate and calculable electrostatic force to the colloidal particle while recording V_{OL}. The technique yields an *in situ* determination of the microscope's OLFS without requiring a determination of either the OLDS, or the cantilever spring constant. Furthermore, we show that the OLDS can be approximated in a noncontact fashion from

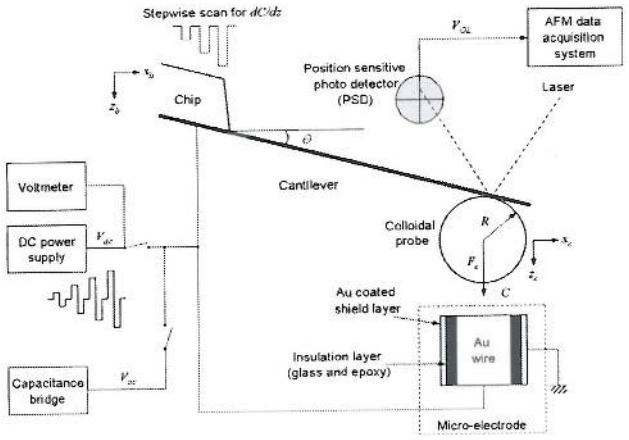

FIG. 2. Schematic of the experimental setup used for the electrostatic calibration that shows the orientation of the colloidal probe with a tilt angle of θ, the position of the probe with respect to the microfabricated electrode, the main displacement coordinates, and the primary signals and measurement instruments.

the thermal noise fluctuations by making use of the known OLFS, in a slight modification of the technique described in Ref. 36. Optical lever force and displacement sensitivities for a range of colloidal probes are determined using our new approaches. An estimate of the spring constant of the colloidal probe is also obtained, which is used in one instance to recalibrate the AFM force sensitivities in an aqueous environment. OLFS values are determined using measurements based on our electrostatic approach $OLFS_E$, a thermal noise technique $OLFS_T$, comparison to a reference cantilever $OLFS_R$, and by comparison to the contact force measured using a calibrated piezoresistive force transducer (PFT) $OLFS_P$ (Refs. 22 and 40) to examine systematic differences among these techniques. We find that calibration approaches requiring contact seem to underestimate the force sensitivity when compared to the benchmark electrostatic value. Finally, correction factors for dynamic mode shape, laser spot size, and laser position,[39] are empirically measured for a thermal method that allows us to compute values of $OLFS_T$ that agree with $OLFS_E$ to within less than 1%.

II. CALIBRATED ELECTROSTATIC FORCE FOR A COLLOIDAL PROBE: PRINCIPLES, GENERAL MEASUREMENT CONSIDERATIONS, METHODS, AND RESULTS

A. Principles

The experiment is illustrated schematically in Fig. 2. The electrostatic force between the probe and the flat end of the microelectrode is expressed as

$$F_e = \frac{1}{2}\frac{dC}{dz_b}(U^2), \tag{2}$$

where F_e is the electrostatic force acting on the probe, dC/dz_b is the capacitance gradient relative to the motion of the cantilever base, and U is the total electrical potential between the two electrodes. Thus, the change in optical lever voltage ΔV_{OL} for a given applied voltage (electrostatic force) can be measured, and the $OLFS_E$ determined using tech-

niques entirely analogous to those described in Ref. 41 for the application of electrostatic forces to a spherical indenter tip.

The OLDS can be computed from the $OLFS_E$ using the thermal noise spectrum as proposed by Higgins *et al.*[36]

$$\mathrm{OLDS} = \sqrt{\frac{\pi k f_R P_{\mathrm{dc}} Q}{2 k_B T}}, \tag{3}$$

where f_R is the resonance frequency, P_{dc} is the dc power response of the cantilever, and Q is the quality factor, all of which are determined from curve fitting of the thermally excited power spectrum of V_{OL} in V^2/Hz (e.g., see Ref. 42), with k_B being the Boltzmann constant and T the temperature of the air surrounding the cantilever. We modify Eq. (3) here by recalling that the displacement and force sensitivities are related by the stiffness [Eq. (1)], so that

$$\mathrm{OLDS}_{ET} = \frac{\pi f_R P_{\mathrm{dc}} Q}{2 k_B T \mathrm{OLFS}_E}, \tag{4}$$

where the subscript on OLDS indicates the value is derived using a combination of electrostatic and thermal based techniques. Equation (4) does not contain correction factors for the difference between the dynamic mode shape and the static deflection, or for the laser spot diameter and its position along the cantilever.[36–39] These corrections are unknown for colloidal probe geometries, but can be estimated from our measurements, as we demonstrate later in the paper.

The presence of electrochemical double layer[43] effects greatly complicates the accurate realization of electrostatic forces in aqueous systems, so direct application of our technique is not always feasible; however, the spring constant can be determined in air by rearranging Eq. (1), so

$$k_E = \frac{\mathrm{OLDS}_{ET}}{\mathrm{OLFS}_E} = \frac{\pi f_R P_{\mathrm{dc}} Q}{2 k_B T \mathrm{OLFS}_E^{\,2}}. \tag{5}$$

This stiffness calculation can be used to recalibrate the probe in a liquid, since the actual stiffness of the sensor is invariant.

B. General measurement considerations

The direct application of a calculable electrostatic force between a sphere and flat was described previously by Chung *et al.*[41] Here, we highlight important differences from this previous work, beginning with the new microcoaxial electrode used to concentrate the electrical field on the now much smaller sphere. Numerical simulations indicate that the microelectrode geometry shown in Fig. 2 can effectively limit the force interaction on spheres as small as 30 μm in diameter. Based on this design analysis, a rigid microcoaxial electrode was fabricated as described in the section that follows. Subsequent attempts to experimentally measure capacitance gradients along the x and y directions, which could skew the electrostatic force from the desired z direction, revealed them to be smaller than could be detected using our equipment.

As illustrated in Fig. 2, the gradient $dC/dz_b \approx \Delta C/\Delta z_b$ is measured using an accurate capacitance bridge to record ΔC while a calibrated displacement sensor records Δz_b, as the probe is moved vertically downward using the AFM's z-axis scan stage. The capacitance is measured at several values of z_b, returning to a home position between each displacement in order to measure and subtract the effects of drift. The deflection of the colloidal probe with respect to the base z_c is negligible during the determination of the gradient, as verified by monitoring the optical lever signal V_{OL}. (This also confirms that surface forces are roughly constant over the considered range of probe surface separations.)

The total electrical potential U between the probe and flat during the dC/dz_b measurement is

$$U = V_{\mathrm{ac}} \sin \omega t + V_s, \tag{6}$$

where V_{ac} is the amplitude of the time varying bridge excitation with angular frequency ω, and V_s is the surface potential. Squaring this total potential and substituting in Eq. (2) we find

$$F_e = \frac{1}{2}\frac{dC}{dz}\left[V_s^{\,2} + \frac{V_{\mathrm{ac}}^2}{2} + 2V_s V_{\mathrm{ac}} \sin \omega t - \frac{V_{\mathrm{ac}}^2}{2}\cos 2\omega t\right]. \tag{7}$$

The net static force terms above cause the cantilever to deflect by a constant amount, since the capacitance gradient is constant to first approximation over the small scan range (<200 nm). The dynamic electrostatic force terms are a source of noise, causing small vibrations of the probe. This noise is minimized by averaging over an integer number of bridge cycles, selecting the smallest V_{ac} that produces a usable signal to noise ratio, and choosing a bridge frequency incommensurate with any of the colloidal probe natural frequencies. V_{OL} is monitored to verify that motions are negligibly small (peak to peak $\Delta V_{\mathrm{OL}} < 2\%$ of the linear V_{OL} range).

After determining the gradient, the capacitance bridge is replaced with a voltage source. A constant potential V_{dc} is applied while the optical lever voltage is measured. The total potential and the resulting electrostatic force in this case are

$$F_e = \frac{1}{2}\frac{dC}{dz}(V_{\mathrm{dc}} + V_s)^2. \tag{8}$$

Working from expressions for both the sum and difference of the electrostatic forces resulting from V_{dc} values of constant magnitude but opposite polarities and using $\mathrm{OLFS}_E = \Delta V_{\mathrm{OL}}/F_e$ to change from F_e to V_{OL} the following quadratic equation is obtained for the surface potential:

$$V_s = |V_{\mathrm{dc}}|\frac{(\sqrt{V_{\mathrm{OL}}^+} - \sqrt{V_{\mathrm{OL}}^-})^2}{V_{\mathrm{OL}}^+ - V_{\mathrm{OL}}^-} \tag{9}$$

where, V_{OL}^+ and V_{OL}^- are the PSD voltages that result from the deflection of the cantilever for application of a fixed V_{dc} of alternately positive and negative polarity, respectively.

C. Methods

A commercial AFM (MFP-3D, Asylum Research, CA) (Ref. 44) was used, where the z-axis of the microscope scanner has a precalibrated linear variable differential transformer displacement transducer. Polystyrene spheres nominally 50 μm in diameter (DRI-CAL Particle Size Standards, Duke Scientific, CA) were attached to five different cantile-

TABLE I. Specifications of the cantilevers and colloidal particles used in the assembly of colloidal probes.

	Cantilever								Colloidal particle	
Colloidal probes no.	Nominal spring constant (N/m)[a]	Shape	Length (μm) [a]	Width (μm) [a]	Thickness (μm) [a]	First resonance frequency f_R (kHz)[b]	Quality factor Q [b]	dc power response P_{dc} (V^2/Hz) [b]	Material	Diameter (μm) [c]
1	42	Rectangular	160	50	4.6	110.018 ± 0.002	438 ± 6	$5.7\times10^{-17}\pm1\times10^{-18}$	Polystyrene with	59
2	42	Rectangular	160	50	4.6	118.833 ± 0.003	530 ± 20	$1.46\times10^{-16}\pm6\times10^{-18}$	Au coating layer	59
3	1.8	Rectangular	240	50	2.8	27.724 ± 0.008	280 ± 30	$1.8\times10^{-14}\pm2\times10^{-15}$		50
4	0.1	Open V-shaped	140	18	0.6	10.889 ± 0.003	98 ± 5	$7.0\times10^{-13}\pm3\times10^{-14}$		58
5	0.01	Open V-shaped	320	22	0.6	2.853 ± 0.001	37.4 ± 0.9	$5.77\times10^{11}\pm8\times10^{-13}$		54
6 (in air)	14	Rectangular	90	35	2	87.424 ± 0.001	434 ± 6	$2.50\times10^{-15}\pm3\times10^{-17}$	Silica glass with	32
6 (in water)						69.64 ± 0.01	8.89 ± 0.07	$4.78\times10^{-13}\pm5\times10^{-15}$	Au coating layer	

[a]The spring constant and the dimensions of the cantilevers are nominal values from the manufacturer.
[b]The resonance frequencies, the quality factors, and the dc power responses of the colloidal probe are determined from the first peak in the thermal noise spectrum. The quoted uncertainty is the standard deviation of ten spectra that were themselves averaged from 50 to 100 separate time series.
[c]The approximate diameter of the colloidal particle is measured using a scanning electron microscope (SEM) image and a calibrated scale.

vers with various nominal spring constants by using conductive epoxy (H21D, Epotek Tech., MA). After curing the epoxy, a Cr adhesion layer was deposited on the assembled colloidal probe followed by a Au layer. The thicknesses of the Cr layer and the Au layer were estimated to be 5 and 30 nm, respectively, using the deposition chamber's microbalance monitoring system. A commercially available conductive colloidal probe with a 32 μm gold coated silica glass sphere (Novascan Technologies, Inc., Ames, IA) was also used. The sphere sizes chosen for this study were selected to be as small as possible while producing measurable capacitance gradients. Table I shows the specifications of the cantilevers that were used in this work. The first resonance frequencies were determined from the first peak in the thermal noise spectra of the PSD output recorded using data acquisition hardware and software available on our AFM. The first modes of the colloidal probes were also fitted to the power response function of a simple harmonic oscillator [see Eq. (1) in Ref. 36] using a least-squares algorithm available on the microscope that allowed us to extract values of the resonance frequency f_R, the dc power response P_{dc}, and the resonance quality factor Q. The diameters of the polystyrene spheres were measured using a scanning electron microscope (SEM) equipped with a calibrated length scale.

The microcoaxial electrode was fabricated using a glass micropipette and a nominal 25 μm diameter gold wire (California Fine Wires, CA). The gold microwire was inserted into the glass micropipette and glued using a nonconductive epoxy. Then, Cr and Au layers were deposited on the resulting assembly by rf and dc sputterings, respectively. The approximate coating thicknesses of the Cr layer and the Au layer were 20 and 400 nm. The end of the Au coated glass micropipette was cut and polished using focused ion beam milling (NVision 40, Zeiss, Germany). Figure 3 shows SEM micrographs of a representative colloidal probe and microelectrode. The diameter of the center electrode is 25 μm and the outer diameter of the electrode is 37 μm.

Capacitance was measured using an Andeen-Hagerling 2700A bridge (AH-bridge, Andeen-Hagerling, Inc., Cleveland, OH). Capacitance measurement is most accurately linked to National Institute of Standards and Technology (NIST) reference standards at an excitation of 1 kHz; hence, this frequency was selected for most of the experiments. However, an excitation of 5 kHz was selected for colloidal probe 5 after considering its 2.853 kHz resonance and observing the 1 kHz forced response magnitude of oscillations at 2 kHz as a result of the 2ω term in Eq. (7). The minimum excitation voltage for the AH bridge is $V_{ac,rms}=1$ V and was chosen for all experiments.

As a general note, the alignment knobs for adjusting the optical lever position on the colloidal probe were fixed after positioning the spot near the end of the cantilever. To measure dC/dz_b, the microelectrode was first centered in the x-y plane beneath the colloidal particle using the AFM sample

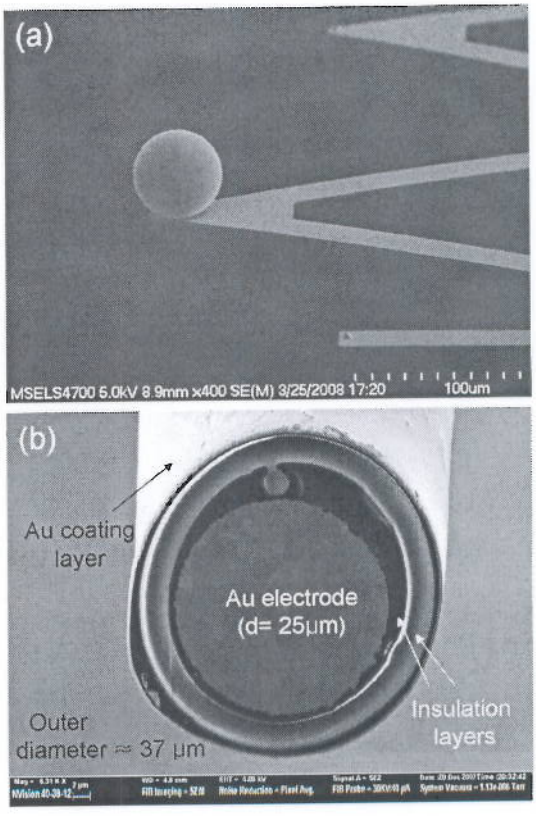

FIG. 3. SEM images of (a) colloidal probe 5 and (b) a tilted, top-down view of the fabricated microelectrode.

stage by maximizing the probe-microelectrode capacitance. The gap between the colloidal particle and the microelectrode surface was set to maintain a precision of a few percent in the measurements of capacitance and displacement changes while avoiding having the colloidal probe jump into contact. Beginning at a fairly large gap, the probe was moved toward the surface in 100 nm increments until a change in capacitance of at least 40 aF was observed. Then, the colloidal probe was retracted back 100 nm, and scanned from this home position along the z-axis toward the electrode in seven steps of 20 nm each. At each step, the capacitance and z_b displacement were measured five times for about 20 s while monitoring V_{OL}. The colloidal probe was moved back to the initial home displacement position between steps to correct for drift. By limiting the total displacement to only 140 nm, the relationship between C and z_b was approximately linear in least-squares curve fits of the data.

The bridge was removed and voltages applied using an external high-voltage power supply, (Model 2350, Tegam Inc., Geneva, OH). The initial gap between the colloidal probe and the electrode was set 20 nm smaller than the previous home position. The applied voltage was measured using an Agilent 3458A (Agilent Technologies, Inc., Loveland, CO) and V_{OL} was monitored using the microscope's data acquisition system. V_{dc} values were selected starting at zero and gradually increasing to yield a total change in PSD output ΔV_{OL} that could be quantified with percent level precision. With practice, it was possible to arrive at a series of V_{dc} increments where the z_c was changing by approximately 20 nm with each electrostatic load. Between the increments, the applied voltage was set back to zero to monitor the baseline and correct for drift. The same voltages with opposite polarities were applied and the surface potential determined using Eq. (9). The experiment was repeated five times for each colloidal probe. After the determination of the force sensitivity, thermal noise spectra were obtained and the OLDS_{ET} was calculated. Ten different thermal noise spectra were obtained by averaging 50 to 100 thermal noise ensembles having bandwidth of 1 MHz with frequency resolutions ranging between 2.38 Hz and 38.146 Hz depending on the natural frequency and quality factor of the vibrational mode being targeted for characterization. The average value of the air temperature around the probe was 28 ± 3 °C as measured using thermocouples included with the AFM.

D. Results

The drift corrected relationship between z_b and capacitance for colloidal probe 4 is given in Fig. 4(a). No systematic residual due to the linear fit is observed in Fig. 4(b). From Fig. 4(c), it can be seen that the deflection and vibration of the cantilever due to the dynamic electrostatic force is less than 2 nm. The average capacitance gradient from the five different measurements using colloidal probe 4 is 0.79 ± 0.04 fF/μm where the stated uncertainty is one standard deviation, and contributions to the uncertainty due to systematic uncertainties in the transfer of the units of length and capacitance were negligible. Throughout the remainder of the paper all uncertainties will be reported in this fashion, unless otherwise noted. The functional relationship between

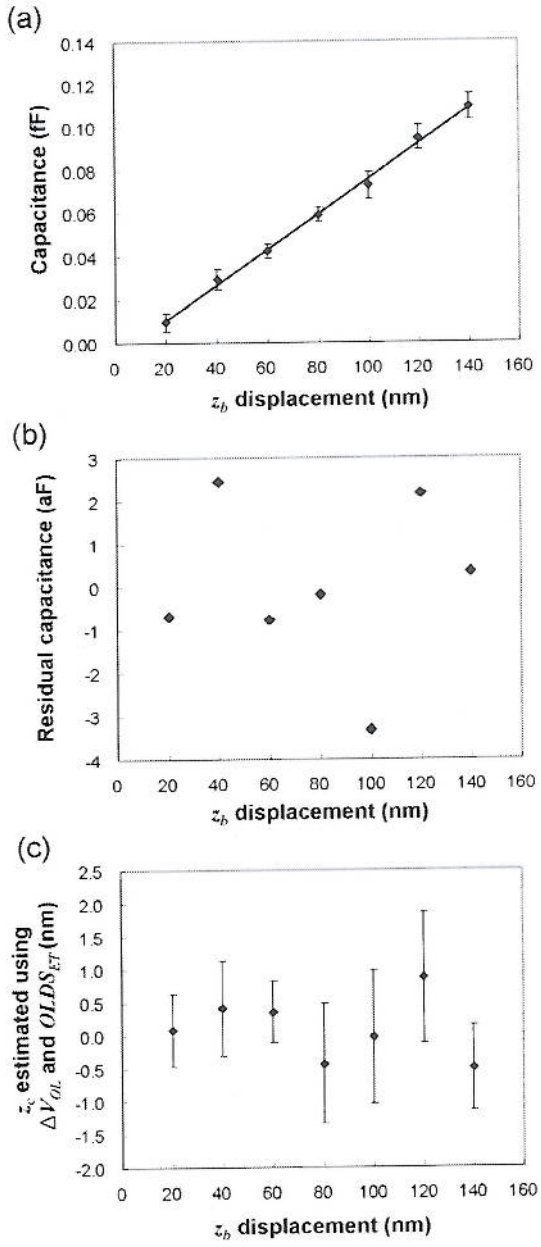

FIG. 4. (Color online) Example of dC/dz_b measurements: (a) linear curve fit of C as a function of z_b, (b) residual capacitance after subtraction of the fit values, and (c) deflection and vibration (error bars) of the cantilever during the capacitance measurement as estimated from the optical lever displacement signal. The data was obtained using colloidal probe 4 with 1 kHz capacitance bridge excitation. The error bars represent one standard deviation of the measured quantities.

the calculated electrostatic force and the corresponding PSD signal is given in Fig. 5. Voltage polarities are distinguished on the plot by open and closed boxes. The resulting surface potential V_s was 0.25 ± 0.03 V. The error bars in Fig. 5 represent estimated uncertainties in the measured quantities. The uncertainty in the measurement of the PSD signal is simply one standard deviation of the voltages measured at a given force increment. The uncertainty in the applied force is derived by propagating the measurement uncertainties associated with the capacitance gradient (which is dominant), the applied voltage, and the surface potential through Eq. (8).

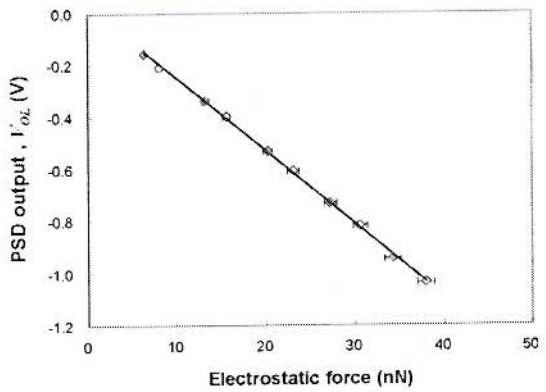

FIG. 5. (Color online) A representative plot of the PSD output as a function of the applied electrostatic force. Data points shown with solid squares correspond to forces applied using negative polarity voltage, and data points shown with empty squares correspond to forces applied using positive polarity voltage. The data were obtained using colloidal probe 4. The error bars of the electrostatic forces represent the uncertainties derived by propagating the measurement uncertainties associated with the capacitance gradient, the applied voltage, and the surface potential.

The applied electrostatic forces ranged from 6.4 ± 0.2 nN to 38 ± 1 nN. The $OLFS_E$ was determined to be 29 ± 1 V/μN using a linear least-squares curve fit to the data of Fig. 5, where the estimated uncertainty is one standard deviation of the $OLFS_E$ values obtained from the five different force curves. From ten thermal noise spectra, the mean value of the $OLDS_{ET}$ was determined to be 9.9 ± 0.8 V/μm. The spring constant k_E was 0.35 ± 0.03 N/m and is computed using Eq. (1), where the total uncertainty is calculated from the individual uncertainties of the optical lever displacement and force sensitivities summed in root mean square fashion. Using the same experimental procedures, the optical lever force and displacement sensitivities of the other colloidal probes were determined. These results as well as estimates of the spring constant for each probe obtained from the electrostatic calibrations are summarized in Table II.

III. OLFS CALIBRATIONS BY OTHER TECHNIQUES

Thermal, reference cantilever, and PFT calibration techniques were completed without moving the optical lever laser spot position on the colloidal probe under test. The principles and methods associated with these other techniques are only briefly reviewed and the reader is directed to the appropriate literature for further details. Spring constants evaluated using the thermal k_T and reference lever k_R techniques are for the probes as they were positioned in the AFM. Reiterating, all spring constants reported in this paper were evaluated in a direction normal to the sample surface without adjustment for tilt.

A. Thermal noise method

The thermal noise method uses the equipartition theorem to relate the Brownian motion of the cantilever to its spring constant.[34] First, $OLDS_C$ is obtained by probing a rigid surface. The probe is then retracted from contact with the surface, and the power spectrum of thermally driven free vibrations measured and curve fit. For consistency, the stiffness was computed by solving Eq. (3) so that

$$k_T = \frac{OLDS_C{}^2 2k_B T}{\pi f_R P_{dc} Q}. \tag{10}$$

This information is then combined to yield the thermal noise method based estimate of the optical lever force sensitivity $OLFS_T = OLDS_C / k_T$. After performing experiments in air, colloidal probe 6 was immersed in de-ionized water for 24 h and the procedures repeated using the fully submerged probe.

$OLDS_C$ values were measured from the slope of V_{OL} versus z_b curves obtained by pressing each probe against a glass microscope slide. The curves were measured in the linear region of the optical lever detection system.[45] Differences in the slopes observed between extension and retraction curves (see Fig. 6) were typically observed to be on the scale of 8%, 1%, 1%, 8%, 12%, and 1% for colloidal probes 1, 2, 3, 4, 5, and 6, respectively. The difference between extension and retraction curves in water was 4% for colloidal probe 6. It is interesting to note that a long range force was observed in Fig. 6(b) for colloidal probe 5, which was probably due to static charge buildup on the nonconductive glass slide. Differences in the slopes are attributed to the sliding friction of the colloidal probe on the surface. In an attempt to compensate for the differences, the mean of the slopes between extension and retraction curves was computed and averaged over ten data sets to arrive at an estimated value of the $OLDS_C$. We find that this estimate agrees with the value obtained using corrections suggested in previous research about the effect of friction on the $OLDS_C$ determination,[27,28] typically within a relative difference of only 0.004.

TABLE II. Experimental results of electrostatic calibration.

Colloidal probes no.	Frequency for capacitance measurement (kHz)	Capacitance gradient dC/dz_b (fF/μm)	Magnitude of maximum applied voltage V_{dc} (V)	Surface potential V_s (V)	Optical lever force sensitivity[a] $OLFS_E$ (V/μN)	Optical lever displacement sensitivity[b] $OLDS_{ET}$ (V/μm)	Electrostatic stiffness k_E (N/m)
1	1	1.61 ± 0.06	110.64	0.1 ± 0.2	0.109 ± 0.006	9.6 ± 0.6	88 ± 8
3	1	1.6 ± 0.3	20.60	0.265 ± 0.009	4.9 ± 0.2	11 ± 1	2.2 ± 0.3
4	1	0.79 ± 0.04	9.40	0.25 ± 0.03	29 ± 1	9.9 ± 0.8	0.35 ± 0.03
5	5	0.41 ± 0.02	3.69	0.34 ± 0.03	300 ± 20	7.8 ± 0.7	0.026 ± 0.003
6	1	1.49 ± 0.09	52.03	0.15 ± 0.02	1.42 ± 0.09	25 ± 2	18 ± 2

[a]The optical lever normal force sensitivity is estimated from direct application of calculable electrostatic forces.
[b]Based on the force sensitivity, the optical lever displacement sensitivity in the direction normal to the sample surface is estimated using supplemental information gained from curve fitting the PSD response to colloidal probe thermal fluctuations.

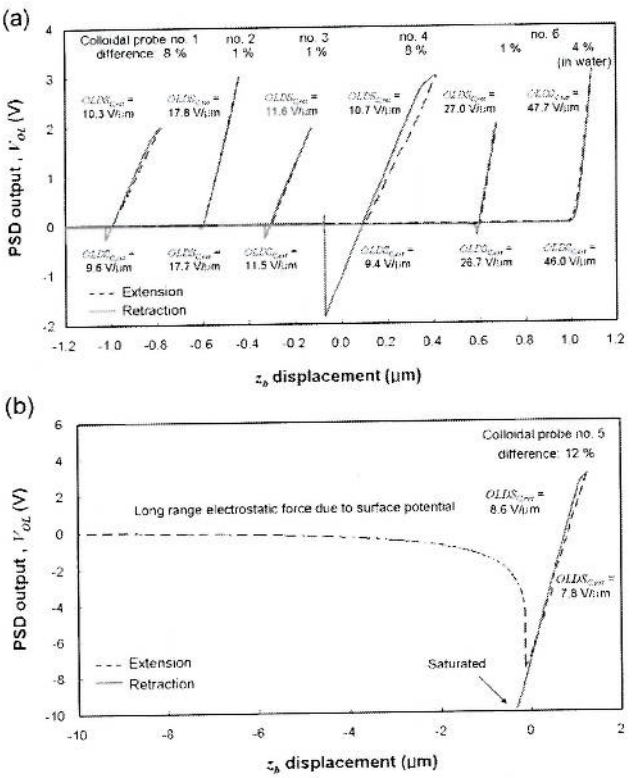

FIG. 6. (Color online) PSD output as a function of AFM z-axis motion when probing a rigid surface formed using a bare glass microscope slide (a) for the colloidal probes 1, 2, 3, 4, and 6 and (b) for the colloidal probe 5. The subscripts *ext* and *ret* denote whether the cantilever is extending toward, or retracting away from the contact surface, respectively. Curves are shown for each colloidal probe considered in the study along with best estimates of the extension and retraction slopes and an expression of the maximum difference between the two estimates $(\mathrm{OLDS}_{\mathrm{ret}}-\mathrm{OLDS}_{\mathrm{ext}})/\mathrm{OLDS}_{\mathrm{ext}}$. For colloidal probe 6 as in (a), the curves in air and in de-ionized water are shown. For the colloidal probe 5 in (b), a long range attractive force is observed due to static charge buildup.

An implicit assumption is that the attached sphere is "rigid" compared to the cantilever stiffness, which may not be the case for polystyrene spheres. In order to evaluate the effect of sphere compliance on the determination of OLDS_C, the contact stiffness of a polystyrene sphere was measured using a commercial instrumented indentation machine (TriboIndenter, Hysitron, Inc., Eden Prairie, MN). A sample was placed in the indentation machine and pressed with a diamond flat punch of 100 μm diameter. The applied force for contact stiffness estimation was 25 μN which was comparable to the force applied during the OLDS_C measurement for colloidal probe 1. The measured stiffness of the sphere was 1.2 ± 0.4 kN/m. This stiffness is only significant in comparison to the nominal value for colloidal probes 1 and 2, and the OLDS_C measurement associated with these probes was corrected using the following relationships:

$$\frac{1}{k_{\mathrm{Meas}}}=\frac{1}{k_T}+\frac{1}{k_{\mathrm{PS}}}, \tag{11}$$

where,

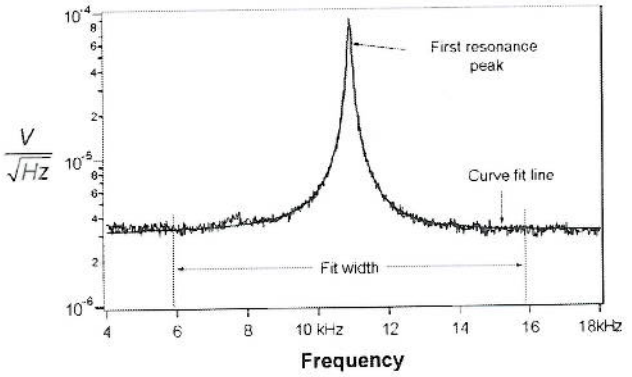

FIG. 7. (Color online) Typical power spectrum of the PSD signal corresponding to thermal-mechanical noise of the colloidal probe. The plot focuses on the resonance peak that is associated with the first mode of vibration and shows typical results of curve fitting a single-mode thermal response function to the raw spectral data. The spectrum shown has 1 MHz total bandwidth and was obtained by processing and averaging 50 individual time series. The parameter fits from ten such plots were averaged to arrive at the estimated thermal parameters, as discussed in the text. Data shown is for colloidal probe 4.

$$k_{\mathrm{Meas}}=\frac{\mathrm{OLDS}_{\mathrm{PS}}^2 2k_bT}{\pi f_r P_{\mathrm{dc}} Q}, \tag{12}$$

k_{PS} is the spring constant of the polystyrene sphere measured using instrumented indentation, and $\mathrm{OLDS}_{\mathrm{PS}}$ is the as measured, or uncorrected contact value of OLDS of colloidal probes 1 and 2. The OLDS_C for probes 1 and 2 was thus computed as

$$\mathrm{OLDS}_C=\mathrm{OLDS}_{\mathrm{PS}}\frac{k_{\mathrm{PS}}}{k_{\mathrm{PS}}-k_{\mathrm{Meas}}}. \tag{13}$$

The thermal noise spectrum was measured from the PSD voltage for the case of free vibrations in air, and, in the one case, for submersion in water. As mentioned previously, correction factors due to dynamic mode shape and laser spot size and location were not used since analytical expressions were not available. The first resonance frequency, background noise level, quality factor, and k_T were determined by curve fitting the noise spectra (see Ref. 42) using software provided as an analysis package on the AFM. The average spring constant was obtained from ten thermal noise spectra, each obtained by processing and averaging 50 to 100 individual time series, and used to compute OLFS_T, the uncertainty of which is expressed as the root mean square sum of the uncertainties in OLDS_C and k_T. Typical data and curve fit are shown in Fig. 7.

B. Calibration by reference cantilever

The reference cantilever method employs a known spring to determine the unknown spring constant of the colloidal probe in a traceable fashion. The optical lever displacement response is obtained by probing both a rigid surface and a reference cantilever with known spring constant. The spring constant of the probe is then determined by[17,20]

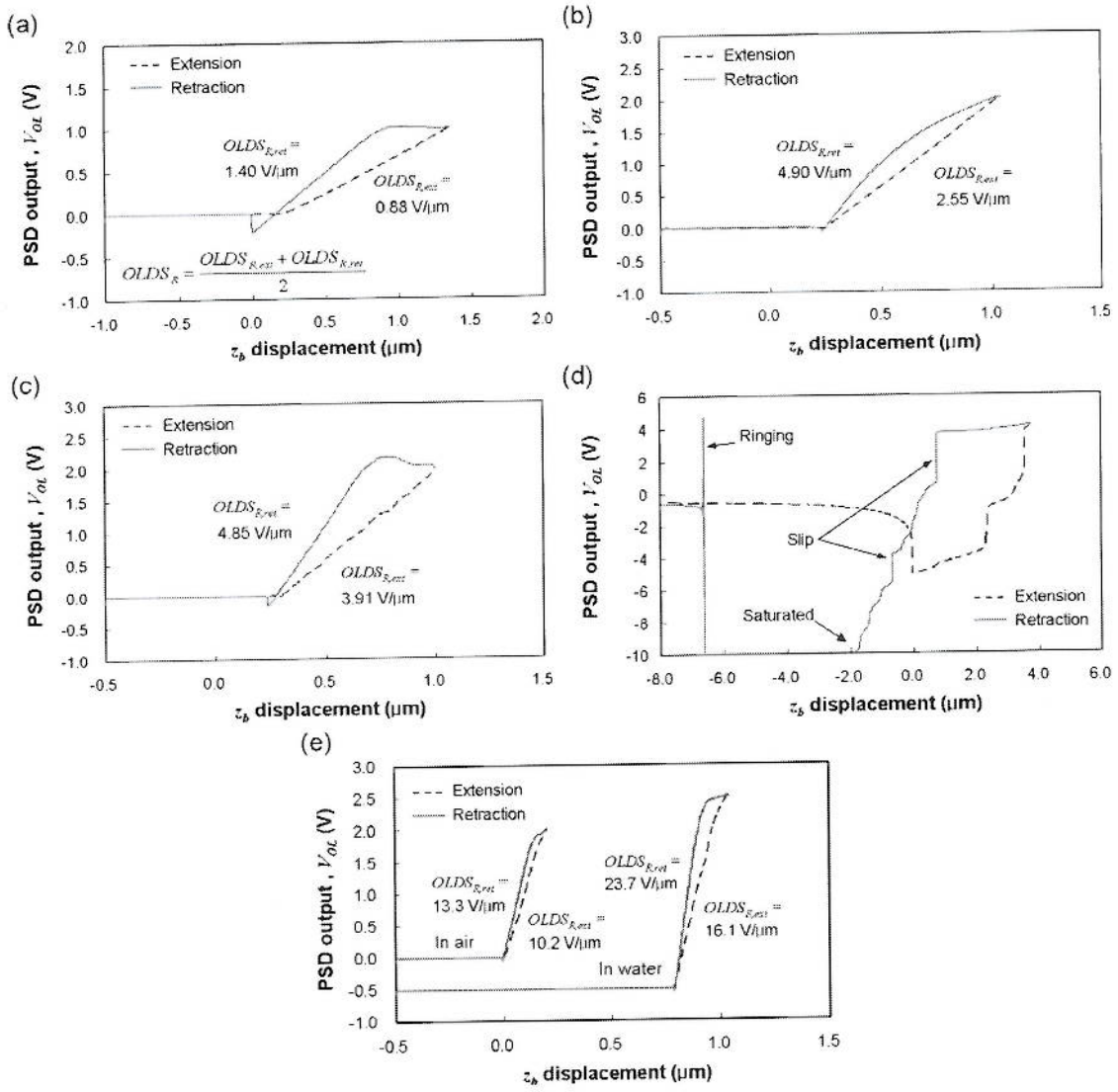

FIG. 8. (Color online) The PSD response observed when probing a reference cantilever with colloidal probes (a) 1, (b) 2, (c) 3, (d) 5, and (d) 6 [the curves for colloidal probe 4 are given in Fig. 1(a)]; The slope of the response curve ($OLDS_R$) is estimated from both the extension and retraction data near the point of zero deflection of the colloidal probe. The mean of these two values is computed as a best estimate of the unconstrained $OLDS_R$. Complex contact friction events dominate the curves shown in (d) and the data was deemed unusable for calibration purposes. Still, the curves in (d) provide clear evidence of sharp transitions that might be characterized as rolling to sliding contact. As for the colloidal probe 6 in (e), the curves in air as well as in de-ionized water are shown.

$$k_R = k_{\text{ref}}\left(\frac{\text{OLDS}_C}{\text{OLDS}_R} - 1\right), \tag{14}$$

where k_R is the spring constant calibrated by using the reference cantilever, k_{ref} is the spring constant of the reference cantilever, and OLDS_R is the optical lever displacement sensitivity that is measured when the probe is pressed against a reference cantilever. The reference cantilever based estimate of the optical lever force sensitivity is then $\text{OLFS}_R = \text{OLDS}_C / k_R$.

All of the reference cantilevers were calibrated using the NIST electrostatic force balance (EFB)[21,46] and were selected to match the nominal stiffness of a corresponding colloidal probe. The reference cantilevers used for colloidal probes 1, 2, 4, 5, and 6 were tipless, whereas the reference cantilever used for colloidal probe 3 had a tip. During the calibration of colloidal probe 3, the lowest position on the colloidal probe could be determined by scanning the colloidal particle using the tip of the reference cantilever. For the other cantilevers, the colloidal probe was carefully aligned along the reference cantilever x axis (along the length) by using a microscope with top and bottom views. The contact point along the x axis could be placed with a precision of approximately 5 μm, and is a major source of uncertainty in this method. The relative uncertainty due to this placement is incorporated into the uncertainty of the tipless cantilevers' stiffness by multiplying the relative uncertainty in reference length by a factor of three to account for the cubic dependence of cantilever stiffness on length. No such additional uncertainty was included for the tipped reference cantilever.

Significant stick-slip events were observed during experiments that used the reference cantilevers with the lowest spring constants, and the general trend of differences be-

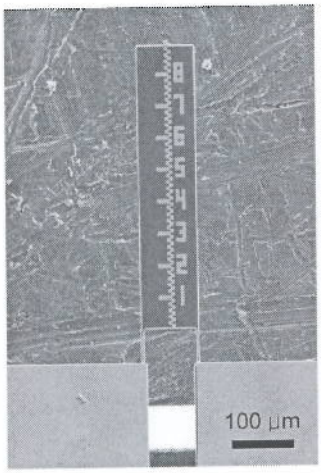

FIG. 9. SEM image of the PFT. The PFT is a cantilever force sensor that uses a piezoresistor to sense changes in loads that can be applied at various prescribed measurement points along its longitudinal axis. The change in resistance for a given contact force was calibrated at each major fiducial point using the NIST EFB as reported previously. (Ref. 40).

tween extension and retraction curves during optical lever displacement calibration was exacerbated, becoming far less deterministic than for the case of probing a rigid surface. When possible, the mean value of the extension and retraction slopes was taken as an estimate of the OLDS_R, with the final reported value for any probe being an average of ten such estimates, and with an uncertainty corresponding to one standard deviation. The reference cantilever based estimate of the probe stiffness was then determined using Eq. (14), which was subsequently used to compute the OLFS_R. The estimated uncertainty of k_R is the root mean square sum of the standard deviation of the ten estimates and the estimated uncertainty of k_{ref}. The uncertainty of OLFS_R was computed as the root mean square sum of uncertainties in k_R and OLDS_C.

Reference cantilever based calibration curves are shown in Fig. 8. The differences between the slopes of the extension and retraction data are obvious. No reliable slopes for colloidal probes 4 and 5 can be discerned from theses curves owing to the large hysteresis and stick-slip events, and no calibration was determined. As shown in Fig. 8(e), colloidal probe 6 was calibrated in air as well as in water by using a reference cantilever. Significant difference was observed in the slopes of extension and retraction curves in liquid. Also, the correction due to the contact stiffness was made for colloidal probes 1 and 2, similar to the OLDS_C determination for the thermal noise method.

C. Calibration by PFT

A PFT, where the resistance depends on the applied force, can also produce a traceable estimate of the force sensitivity.[18,22,40,47,48] The applied force between the colloidal probe and the calibrated PFT can be calculated from a resistance measurement by using the resistance sensitivity S_r of the transducer expressed in Ω/N (or V/N if using a bridge sensor), so that the PFT based estimate of the optical lever force sensitivity OLFS_P is

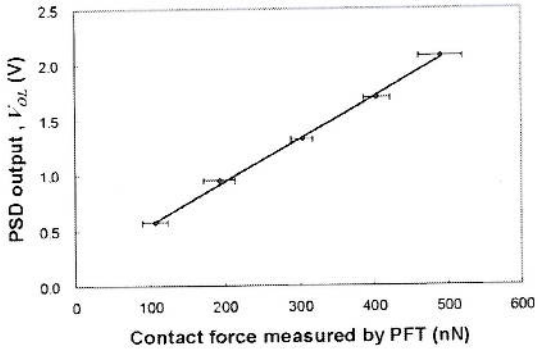

FIG. 10. (Color online) A representative plot of the PSD output as a function of the contact force as measured by the piezoresistive force transducer (PFT). The data shown is for colloidal probe 3. The error bars indicate the standard deviation of the contact force as computed from the change in the resistance of the PFT. The PFT's ability to resolve small changes in force is limited by resistance noise, the force equivalence of which is approximately ± 20 nN. The error bars represent one standard deviation of the measured quantities.

$$\mathrm{OLFS}_P = \frac{S_r \Delta V_{\mathrm{OL}}}{\Delta \Omega}, \tag{15}$$

where $\Delta\Omega$ is the change in the resistance that occurs when the colloidal probe is loaded and unloaded against the transducer.

A picture of the PFT is shown in Fig. 9. The resistance sensitivities and spring constants associated with various points along this device were obtained by using the NIST EFB.[40] The alignment procedure of colloidal probes on the PFT was quite similar to that employed when using reference cantilevers. After alignment, the colloidal probes were pressed against the PFT in five incremental translations. Colloidal probes were unloaded after each step to correct the drift during the deflection and the resistance measurements. The changes in the resistance and the deflection of the probe were monitored at each step. The amount of the deflection of the colloidal probe was carefully selected considering the linear region of the optical lever, the resistance sensitivity of the PFT, and its noise level. The resistance of the PFT was measured using an Agilent 3458A for 10 s at each step (four wire resistance measurements) and noise in this measurement was the dominant uncertainty for probes 4 and 5. The calibration was repeated ten times and the average value of the OLFS_P for each probe was obtained. Positioning inaccuracies produce a relative uncertainty that scales linearly with the estimated uncertainty in contact location (see Ref. 40), and was the dominant source of uncertainty for the case of colloidal probe 2. The total uncertainty is the root mean square sum of this positioning uncertainty with the standard deviation of the ten calibrations. As an example of the calibration by the PFT, the data obtained for colloidal probe 3 is shown in Fig. 10. The colloidal probe spring constant was also evaluated as $k_P = \mathrm{OLDS}_C / \mathrm{OLFS}_P$.

IV. DISCUSSION AND COMPARISON AMONG TECHNIQUES

The OLFS of six different colloidal probes obtained from four different calibration methods along with estimates

TABLE III. Results of colloidal probe sensitivity and spring constant calibrations using thermal, reference cantilever, electrostatic, and piezoresistive force transducer methods without correction.

Colloidal probes no	Optical lever force sensitivity (OLFS) (V/μN)				Optical lever displacement sensitivity (OLDS) (V/μm)		Spring constant (N/m)			
	Electrostatic method $OLFS_E$	Thermal noise method $OLFS_T$	Reference cantilever method $OLFS_R$	Piezoresistive force transducer $OLFS_P$	Dynamic $OLDS_{ET}$	Static $OLDS_C$	Electrostatic method k_E	Thermal noise method k_T	Reference cantilever method k_R	Piezoresistive force transducer k_P
1	0.109 ± 0.006	0.096 ± 0.003	0.104 ± 0.006	...	9.6 ± 0.6	10.84 ± 0.01	88 ± 8	113 ± 3	104 ± 6	...
2	...	0.18 ± 0.01	0.23 ± 0.02	0.18 ± 0.01	...	19.29 ± 0.04	...	107 ± 6	85 ± 6	105 ± 4
3	4.9 ± 0.2	4.6 ± 0.6	4.3 ± 0.3	3.9 ± 0.3	11 ± 1	11.50 ± 0.07	2.2 ± 0.3	2.5 ± 0.3	2.7 ± 0.2	2.9 ± 0.2
4	29 ± 1	28 ± 3	...	24 ± 4	9.9 ± 0.8	10.3 ± 0.3	0.35 ± 0.03	0.37 ± 0.03	...	0.44 ± 0.08
5	300 ± 20	290 ± 10	...	200 ± 50	7.8 ± 0.7	8.2 ± 0.1	0.026 ± 0.003	0.029 ± 0.001	...	0.04 ± 0.01
6 (in air)	1.42 ± 0.09	1.34 ± 0.03	1.4 ± 0.2	...	25 ± 2	26.8 ± 0.1	18 ± 2	20.0 ± 0.4	20 ± 3	...
6 (in water)	...	2.39 ± 0.05	2.2 ± 0.4	...	...	46.7 ± 0.3	...	19.5 ± 0.4	21 ± 4	...

of the combined uncertainties associated with each evaluation are given in Table III. Also determined were estimates of the OLDS using the contact based approach along with the dynamic estimate $OLDS_{ET}$ from Eq. (4) using $OLFS_E$ and parameters identified in the thermal spectra of V_{OL}. Values for the probe spring constants were also determined in many instances, and are presented in the table for reference.

A. OLFS results

The traceable determinations of the OLFS (electrostatic, reference cantilever, and PFT) agreed to within the expanded measurement uncertainty associated with a 95% confidence interval. Uncertainties for the contact based measurements were fairly large, in general due to difficulties in determining the exact point of contact for reference cantilever experiments, and due to limitations of the force resolution of the PFT when testing probes 4 and 5. Certain systematic trends are apparent in the overall data. OLFS values determined from the electrostatic force calibrations are larger than those obtained using the thermal, reference cantilever, and PFT based techniques. Because the noncontact calibration using electrostatic force imposes no physical constraint on the sensing element, it should yield an unbiased estimate of the force sensitivity of the AFM, barring an unaccounted for systematic error source. It is also based on a traceable measurement chain (i.e., all supporting calibrations are referenced to standards that have known values and uncertainties, consistent with the definitions and conventions of the International System of Units). From this standpoint, $OLFS_E$ represents the most accurate determination of the colloidal probe force sensitivity in this set of experiments, and is used as the benchmark. All other methods considered in this study require contact between the probe and a surface during some portion of the calibration and are potentially biased, as discussed next.

Previous friction studies[25–28] have concluded that the colloid probe slides along the surface due to the cantilever tilt as shown in Fig. 11, and that the resulting tangential force has the character of sliding friction; it is proportional to the normal force, but directed in opposition to the motion. This sliding friction produces a torque that opposes the normal bending moment, and is proportional to the probe displacement. The net result of such a force is to make the colloidal probe appear stiffer during an extension curve than for unconstrained motion (e.g., smaller OLFS), as discussed in Refs. 26 and 27 for the case of probing against a rigid surface. The clearest evidence of this behavior is in the plot of Fig. 8(c). Two linear, yet different slopes are evident in this plot, that are separated by a region where the optical lever signal changes little in response to the retraction of the probe stage. The $OLFS_R$ estimated from the extension data is 3.7 V/μN, whereas the value estimated from the retraction data is 5.2 V/μN. These two estimates bracket in magnitude the value identified using the electrostatic technique, which was 4.9 V/μN. Assuming the effect of friction is equal, but opposite between approach and retraction data, the mean of the extension and retraction estimates was evaluated in an attempt to compensate for the bias. Apparently, the friction effect in this case was not completely symmetric, because the

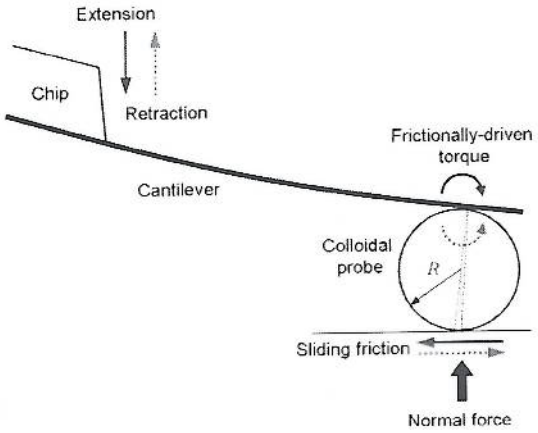

FIG. 11. (Color online) Schematic of the net normal and friction forces acting on the colloidal probe for contact conditions with sliding.

mean value of 4.5 $V/\mu N$ underestimates the OLFS by approximately 10% with respect to the electrostatic determination.

The largest bias between techniques appears in the results for colloidal probe 5, where the calibration using the PFT gives a value of the $OLFS_P$ that is approximately 30% lower than that obtained using the electrostatic force. In fact, $OLFS_P$ values are consistently the smallest estimate of the true OLFS in each of the probes investigated. A possible explanation for this trend is that the procedure for $OLFS_P$ calibration consisted of only extension and not retraction data.

Finally, both a contact and a noncontact value of the $OLFS_T$ were determined for colloidal probe 6 while submerged in a fluid (only the contact result is reported in Table III). To compute the noncontact value, a corrected estimate of k from the electrostatic calibration (19 ± 2 N/m) was determined in air using Eq. (5) (the correction will be discussed in the following section). The probe was then submerged, the optical lever realigned, and a noncontact estimate of OLDS $=46 \pm 2$ $V/\mu m$ (mean $\pm$ combined uncertainty) obtained from Eq. (3) using parameters from a fit of the probe thermal response in the fluid. The OLFS computed by plugging values into Eq. (1) was then 2.4 ± 0.2 $V/\mu N$. For comparison, the $OLFS_T$ of the submerged cantilever was also calculated using the same thermal spectrum parameters and a displacement sensitivity measured yielding $OLDS_C$ $=46.7 \pm 0.3$ $V/\mu m$ (general discrepancies between contact and noncontact estimates of the OLDS are taken up in the next section). OLFS using this combination was 2.39 ± 0.05 $V/\mu N$, while the value determined using the reference cantilever, $OLFS_R$ was 2.2 ± 0.4 $V/\mu N$. All three values agree to within the experimental uncertainty.

B. OLDS results

Each $OLDS_{ET}$ value is lower than its $OLDS_C$ counterpart. We rule out a difference introduced by the frictionally driven torque for colloidal probes 2, 3, and 6 (in air) because in the data of Fig. 6 the relative difference in slopes between extension and retraction curves is about 1%. Therefore, for colloidal probes 2, 3, and 6 (in air) at least, $OLDS_C$ seems the best estimate of the true value. However, if this is the true displacement sensitivity, then $OLFS_T$ for colloidal probe 3 should agree with $OLFS_E$ to within the measurement uncertainty, provided the underlying model of the thermal response function is correct. Recall that in determining an expression for $OLFS_T$, correction factors for dynamic mode shape and laser spot size and location along the cantilever portion of the probe were neglected. By combining these corrections, Eq. (4) can be restated as

$$\mathrm{OLDS}_{ET\ \mathrm{corr}} = \frac{\alpha \pi f_R P_{\mathrm{dc}} Q}{2 k_B T \mathrm{OLFS}_E}, \tag{16}$$

where α is a multiplicative correction factor that accounts for both the dynamic mode shape and the laser spot size effects. The value of α for colloidal probe 3 is 1.07, based on the ratio of the $OLDS_C$ to the uncorrected $OLDS_{ET}$ in Table III. This geometric correction factor must also be used in the determination of k_T, or from Eq. (10)

$$k_{T\ \mathrm{corr}} = \frac{\mathrm{OLDS}_C{}^2 2 k_B T}{\alpha \pi f_R P_{\mathrm{dc}} Q}, \tag{17}$$

so that the value of $OLFS_T$ reported in Table III should be corrected upwards by a factor of α, or $OLFS_{T\ \mathrm{corr}}$ $=4.9$ $V/\mu N$ for colloidal probe 3 which then agrees with our estimate of $OLFS_E$ to within measurement uncertainty. Likewise, $OLDS_{ET\ \mathrm{corr}}$, can be calculated by multiplication of α with $OLDS_{ET}$, thereby allowing the calculation of a corrected $k_{E\ \mathrm{corr}}$, based on Eq. (6).

Table IV summarizes the various empirical values of α, along with the corrected values $OLFS_{T\ \mathrm{corr}}$, $k_{E\ \mathrm{corr}}$, and $k_{T\ \mathrm{corr}}$. The empirically based estimate for the correction between static and dynamic displacement sensitivity can only be achieved by pressing the probe under test against a rigid surface, which compromises the goal of achieving a com-

TABLE IV. Results after applying an empirical estimate of the geometric correction term α to reconcile differences caused by dynamic vs static determination of the OLDS.

Colloidal probes no.	Correction factor α	Optical lever force sensitivity by thermal noise method after correction $OLFS_{ET\ \mathrm{corr}}$ ($V/\mu N$)	Electrostatic spring constant after correction $k_{E\ \mathrm{corr}}$ (N/m)	Thermal spring constant after correction $k_{T\ \mathrm{corr}}$ (N/m)
1	1.13	0.108 ± 0.003	99 ± 8	100 ± 3
3	1.07	4.9 ± 0.6	2.3 ± 0.3	2.4 ± 0.3
4	1.04	29 ± 3	0.36 ± 0.03	0.36 ± 0.03
5	1.05	300 ± 10	0.027 ± 0.003	0.027 ± 0.001
6	1.06	1.42 ± 0.03	19 ± 2	18.9 ± 0.4

pletely noncontact calibration. We note that the values of α computed in air are quite close to a previously reported correction factor (1.09) used for regular AFM cantilevers, assuming a small laser spot focused at the far distal end of a rectangular cantilever.[36] In fact, the mean of the correction factors determined here is 1.07, so that general adoption of 1.09 as a correction factor for colloidal probes operating in air would lead to systematic errors of at most 5% within the broad range of cantilever geometries considered in this study.

A similar approach can be followed for a colloidal probe in an aqueous environment. Based on the corrected spring constant of colloidal probe 6 from the electrostatic calibration in Table IV (19 ± 2 N/m), the OLDS of the same probe when submerged in de-ionized water was calculated from the thermal noise spectra to be 46 ± 2 V/μm (mean $\pm$ combined uncertainty) using Eq. (3). Comparing this value to the OLDS_C determined in water (46.7 ± 0.3 V/μm), a correction factor was determined to be 1.02. It is interesting to note that the empirically based correction for operation in fluid is less than that observed in air ($\alpha = 1.06$) with all other parameters being similar. The difference is indirect evidence of a slight change in the dynamic mode shape between the two environments. This method allows a full recalibration of the colloidal probe measurement parameters in fluid from the spring constant determined in air.

V. CONCLUSIONS

The optical lever displacement and force sensitivity of AFMs equipped with colloidal probes are difficult to calibrate accurately. Here, we have demonstrated a noncontact technique that provides an accurate means of determining the force sensitivity of conductive colloidal probe AFM. This method involves the application of an SI-traceable electrostatic force to the colloidal particle at the end of the cantilever using a microelectrode. The new method allows a direct and accurate determination of the AFM force sensitivity, OLFS, which was used here as a benchmark to evaluate the accuracy of other more convenient methods. Furthermore, electrostatic calibration results were combined with measurements of the AFM thermal noise spectra to estimate other physical parameters of interest, such as the optical lever sensitivity and the cantilever stiffness. Results were contrasted with those obtained using more conventional calibration approaches, and the influence of the frictional torque on colloidal probe measurements was apparent. In particular, OLDS values estimated from contact with both rigid and compliant reference surfaces were found to depend in a systematic fashion on whether the OLDS was computed using extension or retraction data. The observed dependencies when probing against rigid surfaces were consistent with a previous study[27,28] aimed at measuring friction. It was found that the accuracy of reference cantilever based calibration can be improved by computing the mean OLFS between extension and retraction data, although discrepancies persist, and a model for the frictional torque interaction seems necessary if accuracy is to be further improved. The electrostatic force sensitivity was also used to evaluate the accuracy of a far more convenient thermal noise calibration method. A single empirical correction factor α for the combined effects of the unknown mode shape, and beam diameter and placement was developed for the thermal noise method by observing discrepancies between the static estimate of the optical lever sensitivity obtained from constant compliance curves and the dynamically determined estimate based on the electrostatic force sensitivity and thermal noise spectrum. Such geometric correction factors are analytically difficult to determine for colloidal probes. Here, the empirical evaluations of this constant ranged only between 1.04–1.13, so that it appears one can assume a value of 1.09 for a wide variety of probes and reasonably expect this correction to yield thermal based estimates of the normal force sensitivity to within a few percent (<5%) of the true value, provided the OLDS is estimated using the mean of extension and retraction data from a rigid surface.

ACKNOWLEDGMENTS

The authors would like to thank Dr. Bin Ming and Mr. Richard Kasica from NIST for Focused Ion Beam machining of the microelectrode. Piezoresistive force transducers were fabricated by Dr. John Moreland of NIST. The simulations of microelectrode performance by Dr. Rae-Duk Lee were also greatly appreciated. We also acknowledge the help of Dr. Chang-Hwa Lee and Dr. Andras Vladar from NIST for SEM images and Dr. Mark Reitsma for the nanoindentation on the polystyrene sphere.

[1] G. Binnig, C. F. Quate, and C. Gerber, Phys. Rev. Lett. **56**, 930 (1986).
[2] N. A. Burnham and R. J. Colton, J. Vac. Sci. Technol. A **7**, 2906 (1989).
[3] U. Mohideen and A. Roy, Phys. Rev. Lett. **81**, 4549 (1998).
[4] W. A. Ducker, T. J. Senden, and R. M. Pashley, Nature (London) **353**, 239 (1991).
[5] D. P. McDaniel, G. A. Shaw, J. T. Elliott, K. Bhadriraju, C. Meuse, K. H. Chung, and A. L. Plant, Biophys. J. **92**, 1759 (2007).
[6] H. J. Butt, Biophys. J. **60**, 1438 (1991).
[7] L. O. Heim, J. Blum, M. Preuss, and H. J. Butt, Phys. Rev. Lett. **83**, 3328 (1999).
[8] J. Grobelny, N. Pradeep, D. I. Kim, and Z. C. Ying, Appl. Phys. Lett. **88**, 091906 (2006).
[9] R. E. Mahaffy, C. K. Shih, F. C. MacKintosh, and J. Kas, Phys. Rev. Lett. **85**, 880 (2000).
[10] G. Meyer and N. M. Am, Appl. Phys. Lett. **53**, 1045 (1988).
[11] S. Alexander, L. Hellemans, O. Marti, J. Schneir, V. Elings, P. K. Hansma, M. Longmire, and J. Gurley, J. Appl. Phys. **65**, 164 (1989).
[12] S. A. Edwards, W. A. Ducker, and J. E. Sader, J. Appl. Phys. **103**, 064513 (2008).
[13] C. A. Clifford and M. P. Seah, Nanotechnology **16**, 1666 (2005).
[14] V. S. J. Craig and C. Neto, Langmuir **17**, 6018 (2001).
[15] P. J. Cumpson and J. Hedley, Nanotechnology **14**, 1279 (2003).
[16] R. S. Gates and J. R. Pratt, Meas. Sci. Technol. **17**, 2852 (2006).
[17] R. S. Gates and M. G. Reitsma, Rev. Sci. Instrum. **78**, 086101 (2007).
[18] M. S. Kim, J. H. Choi, Y. K. Park, and J. H. Kim, Metrologia **43**, 389 (2006).
[19] E. D. Langlois, G. A. Shaw, J. A. Kramar, J. R. Pratt, and D. C. Hurley, Rev. Sci. Instrum. **78**, 093705 (2007).
[20] A. Torii, M. Sasaki, K. Hane, and S. Okuma, Meas. Sci. Technol. **7**, 179 (1996).
[21] J. R. Pratt, J. A. Kramar, D. B. Newell, and D. T. Smith, Meas. Sci. Technol. **16**, 2129 (2005).
[22] J. R. Pratt, D. T. Smith, D. B. Newell, J. A. Kramar, and E. Whitenton, J. Mater. Res. **19**, 366 (2004).
[23] J. H. Hoh and A. Engel, Langmuir **9**, 3310 (1993).
[24] J. A. Ruan and B. Bhushan, ASME J. Tribol. **116**, 378 (1994).
[25] R. J. Warmack, X. Y. Zheng, T. Thundat, and D. P. Allison, Rev. Sci. Instrum. **65**, 394 (1994).

[26] P. Attard, A. Carambassis, and M. W. Rutland, Langmuir **15**, 553 (1999).
[27] J. Stiernstedt, M. W. Rutland, and P. Attard, Rev. Sci. Instrum. **76**, 083710 (2005).
[28] J. Stiernstedt, M. W. Rutland, and P. Attard, Rev. Sci. Instrum. **77**, 019901 (2006).
[29] C. E. McNamee, N. Pyo, and K. Higashitani, Biophys. J. **91**, 1960 (2006).
[30] S. L. McGurk, R. J. Green, G. H. W. Sanders, M. C. Davies, C. J. Roberts, S. J. B. Tendler, and P. M. Williams, Langmuir **15**, 5136 (1999).
[31] K. E. Bremmell, P. Kingshott, Z. Ademovic, B. Winther-Jensen, and H. J. Griesser, Langmuir **22**, 313 (2006).
[32] J. E. Sader, J. Pacifico, C. P. Green, and P. Mulvaney, J. Appl. Phys. **97**, 124903 (2005).
[33] J. P. Cleveland, S. Manne, D. Bocek, and P. K. Hansma, Rev. Sci. Instrum. **64**, 403 (1993).
[34] J. L. Hutter and J. Bechhoefer, Rev. Sci. Instrum. **64**, 1868 (1993).
[35] G. A. Matei, E. J. Thoreson, J. R. Pratt, D. B. Newell, and N. A. Burnham, Rev. Sci. Instrum. **77**, 083703 (2006).
[36] M. J. Higgins, R. Proksch, J. E. Sader, M. Polcik, S. Mc Endoo, J. P. Cleveland, and S. P. Jarvis, Rev. Sci. Instrum. **77**, 013701 (2006).
[37] P. Attard, T. Pettersson, and M. W. Rutland, Rev. Sci. Instrum. **77**, 116110 (2006).
[38] H. J. Butt and M. Jaschke, Nanotechnology **6**, 1 (1995).
[39] R. Proksch, T. E. Schaffer, J. P. Cleveland, R. C. Callahan, and M. B. Viani, Nanotechnology **15**, 1344 (2004).
[40] J. R. Pratt, J. A. Kramar, G. A. Shaw, D. T. Smith, and J. M. Moreland, Proceedings of the MRS Spring Meeting, San Francisco, CA, 2007 (unpublished), Vol. 1021, pp. HH1002.
[41] K. H. Chung, S. Scholz, G. A. Shaw, J. A. Kramar, and J. R. Pratt, Rev. Sci. Instrum. **79**, 095105 (2008).
[42] D. A. Walters, J. P. Cleveland, N. H. Thomson, P. K. Hansma, M. A. Wendman, G. Gurley, and V. Elings, Rev. Sci. Instrum. **67**, 3583 (1996).
[43] J. Frechette and T. K. Vanderlick, Langmuir **17**, 7620 (2001).
[44] Commercial equipment and materials are identified in order to adequately specify certain procedures. In no case does such identification imply recommendation or endorsement by the National Institute of Standards and Technology, nor does it imply that the materials or equipment identified are necessarily the best available for the purpose.
[45] E. C. C. M. Silva and K. J. Van Vliet, Nanotechnology **17**, 5525 (2006).
[46] D. B. Newell, J. A. Kramar, J. R. Pratt, D. T. Smith, and E. R. Williams, IEEE Trans. Instrum. Meas. **52**, 508 (2003).
[47] S. B. Aksu and J. A. Turner, Rev. Sci. Instrum. **78**, 043704 (2007).
[48] I. Behrens, L. Doering, and E. Peiner, J. Micromech. Microeng. **13**, S171 (2003).